

# CCD *UBV* photometry of the open cluster NGC 6819

T. Ak<sup>1</sup> • Z. F. Bostancı<sup>1</sup> • T. Yontan<sup>2</sup> • S. Bilir<sup>1</sup>  
 • T. Güver<sup>1</sup> • S. Ak<sup>1</sup> • H. Ürgüp<sup>2</sup> • E. Paunzen<sup>3</sup>

**Abstract** We present the results of CCD *UBV* observations of the open cluster NGC 6819. We calculated the stellar density profile in the cluster’s field to determine the structural parameters of NGC 6819. Using the existing astrometric data, we calculated the probabilities of the stars being physical members of

the cluster, and used these objects in the determination of the astrophysical parameters of NGC 6819. We inferred the reddening and metallicity of the cluster as  $E(B - V) = 0.130 \pm 0.035$  mag and  $[Fe/H] = +0.051 \pm 0.020$  dex, respectively, using the  $U - B$  vs  $B - V$  two-colour diagram and UV excesses of the F-G type main-sequence stars. We fit the colour-magnitude diagrams of NGC 6819 with the PARSEC isochrones and derived the distance modulus, distance and age of the cluster as  $\mu_V = 12.22 \pm 0.10$  mag,  $d = 2309 \pm 106$  pc and  $t = 2.4 \pm 0.2$  Gyr, respectively. The parameters of the galactic orbit estimated for NGC 6819 indicate that the cluster is orbiting in a slightly eccentric orbit of  $e = 0.06$  with a period of  $P_{orb} = 142$  Myr. The slope of the mass function estimated for the cluster is close to the one found for the stars in the solar neighbourhood.

**Keywords** Galaxy: open cluster and associations: individual: NGC 6819 – stars: Hertzsprung Russell (HR) diagram

T. Ak

<sup>1</sup>Istanbul University, Faculty of Science, Department of Astronomy and Space Sciences, 34119 University, Istanbul, Turkey

Z. F. Bostancı

<sup>1</sup>Istanbul University, Faculty of Science, Department of Astronomy and Space Sciences, 34119 University, Istanbul, Turkey

T. Yontan

<sup>1</sup>Istanbul University, Graduate School of Science and Engineering, Department of Astronomy and Space Sciences, 34116, Beyazıt, Istanbul, Turkey

S. Bilir

<sup>1</sup>Istanbul University, Faculty of Science, Department of Astronomy and Space Sciences, 34119 University, Istanbul, Turkey

T. Güver

<sup>2</sup>Istanbul University, Faculty of Science, Department of Astronomy and Space Sciences, 34119 University, Istanbul, Turkey

S. Ak

<sup>2</sup>Istanbul University, Faculty of Science, Department of Astronomy and Space Sciences, 34119 University, Istanbul, Turkey

H. Ürgüp

<sup>1</sup>Istanbul University, Graduate School of Science and Engineering, Department of Astronomy and Space Sciences, 34116, Beyazıt, Istanbul, Turkey

E. Paunzen

<sup>3</sup>Department of Theoretical Physics and Astrophysics, Masaryk University, Kotlářská 2, 611 37 Brno, Czech Republic

## 1 Introduction

NGC 6819 ( $\alpha_{2000.0} = 19^h41^m18^s$ ,  $\delta_{2000.0} = +40^\circ11'12''$ ; WEBDA database<sup>1</sup>) is a well-known intermediate age ( $\sim 2.3$  Gyr) open cluster in the Kepler field (Borucki et al. 2011). Its age and location in the Kepler field makes it one of the most suitable clusters for investigating stellar models and for astroseismic studies of stars in different stages of their evolution. The colour excesses, distance moduli, distances, ages, metallicities and radial velocities obtained for NGC 6819 in the previous studies are summarized in Table 1.

NGC 6819 has also often been monitored for stellar seismological studies and to search for variable

<sup>1</sup>webda.physics.muni.cz

**Table 1** Colour excesses ( $E(B - V)$ ), distance moduli ( $\mu_V$ ), distances ( $d$ ), ages ( $t$ ) and metallicities ( $[Fe/H]$ ) collected from the literature for the open cluster NGC 6819. References are given in the last column.

$E(B - V)$ (mag)	$\mu_V$ (mag)	$d$ (kpc)	$t$ (Gyr)	$[Fe/H]$ (dex)	$V_r$ (km s $^{-1}$ )	Refs.
0.12	–	2.04	4.0	$-0.02 \pm 0.02$	–	1
0.30	–	2.2	2	–	–	2
0.28	–	2.17	2	–	–	3
0.16	–	–	2.4	$-0.05$	–	4
$0.14 \pm 0.04$	–	–	–	$+0.09 \pm 0.03$	–	5
0.10	$12.30 \pm 0.12$	2.5	–	–	–	6
$0.10 \pm 0.03$	$12.11 \pm 0.20$	2.3	$2.5 \pm 0.6$	$+0.07$	–	7
0.15	$12.32 \pm 0.05$	2.3	$2.5 \pm 0.6$	$+0.07$	–	8
$0.14 \pm 0.04$	$12.36 \pm 0.10$	2.4	2.6	$+0.09$	–	9
0.15	$12.20 \pm 0.06$	2.2	2.5	$+0.11$	–	10
0.12	$12.27 \pm 0.01$	2.4	–	–	–	11
$0.160 \pm 0.007$	$12.40 \pm 0.12$	2.4	$2.3 \pm 0.2$	$-0.06 \pm 0.04$	–	12
–	–	–	$2.25 \pm 0.20$	–	–	13
–	–	–	–	–	$-7 \pm 13$	14
–	–	–	–	$+0.05 \pm 0.11$	–	15
–	–	–	–	–	$+4.8 \pm 0.9$	16
–	–	–	–	–	$+1 \pm 6$	17
0.10	12.30	2.5	2.4	0	$+2.34 \pm 0.05$	18
–	–	–	–	$-0.02 \pm 0.02$	$+2.65 \pm 1.36$	19

(1) Burkhead (1971), (2) Lindoff (1972), (3) Auner (1974), (4) Rosvick & Vandenberg (1998), (5) Bragaglia et al. (2001), (6) Kalirai et al. (2001), (7) Kang & Ann (2002), (8) Basu et al. (2011), (9) Yang et al. (2013), (10) Balona et al. (2013), (11) Rodrigues et al. (2014), (12) Anthony-Twarog et al. (2014), (13) Bedin et al. (2015), (14) Friel et al. (1989), (15) Friel & Janes (1993), (16) Glushkova et al. (1993), (17) Thogersen et al. (1993), (18) Hole et al. (2009), (19) Lee-Brown et al. (2015).

stars (e.g., Street et al. 2005; Talamantes et al. 2010; Basu et al. 2011; Hekker et al. 2011; Stello et al. 2011; Miglio et al. 2012; Corsaro et al. 2012; Sandquist et al. 2013; Wu et al. 2014a,b). Note that Gosnell et al. (2012) discovered X-ray sources within the cluster’s half-light radius. Although detailed photometric analysis of a cluster is very important to study the stellar models, spectroscopic study of the members of a cluster can give valuable information for the metallicity and radial velocity of the cluster (see Table 1). Recently, Lee-Brown et al. (2015) analyzed high-dispersion spectra of 333 stars in NGC 6819 to determine the abundances of iron and other metals from spectral features in the 400 Å region surrounding the Li 6708 Å line. They found its metallicity to be  $[Fe/H] = -0.02 \pm 0.02$  dex using a sub-sample restricted to main-sequence and turnoff stars.

Here, we report the results of CCD  $UBV$  observations of the open cluster NGC 6819 since it is located in the Kepler field (Borucki et al. 2011) and the mean radial velocity and metallicity of the cluster is determined from the high resolution spectra of a considerable number of cluster’s members brighter than  $V \sim 16.7$  mag

(Lee-Brown et al. 2015). The availability of photometric and spectroscopic data encouraged us to re-calculate the cluster’s astrophysical and kinematical parameters.

We calculate the membership probabilities of the stars in the cluster’s field based on their proper motions and the mean radial velocity of the cluster. We find the reddening and metallicity of NGC 6819 following two independent methods. We infer its distance modulus and age by fitting stellar isochrones to the observed CMDs of the cluster, while keeping the reddening and metallicity constant (Yontan et al. 2014; Bostancı et al. 2015). With this method, we believe that the parameter degeneracy/indeterminacy in the simultaneous statistical solutions (cf. Anders et al. 2004; King et al. 2005; Bridžius et al. 2008; de Meulenaer et al. 2013; Janes et al. 2014) of the astrophysical parameters of NGC 6819 can be reduced.

In Section 2, we summarize the observations and reductions. We present the CMDs, structural parameters of NGC 6819, and the membership probabilities of the stars in the cluster field in Section 3. In section 4, we measure the astrophysical parameters of the cluster. We summarize our conclusions in Section 5.

## 2 Observations

CCD *UBV* observations of the open cluster NGC 6819 were carried out on 18th May 2015 using the 1m Ritchey-Chrétien telescope (T100) of the TÜBİTAK National Observatory (TUG)<sup>2</sup> located in Bakırtepe, Antalya/Turkey. The telescope is equipped with an SI 1100 CCD camera (back illuminated, 4k×4k pixels) operating at −90 deg C. Overall the imaging system has a pixel scale of 0."31 pixel<sup>−1</sup>, resulting in a total field of view of about 21' × 21'. The readout noise and gain of the CCD are 4.19e<sup>−</sup> and 0.55 e<sup>−</sup>/ADU, respectively. The field of the cluster was observed using both short and long exposures in each filter in order to be able to cover the widest possible flux range. Log of observations is given in Table 2. The night was moderately photometric with a mean seeing of 1".6. A *V*-band image taken with an exposure time of 360s is shown in Fig. 1.

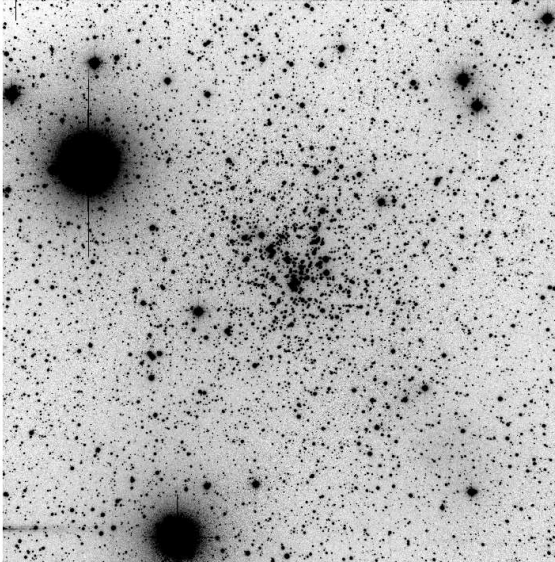


**Fig. 1** A 360 second *V*-band image of NGC 6819 obtained with T100 telescope of the TÜBİTAK National Observatory. The image is given in inverse colour. The field of view is about 21×21 arcmin (North top and East left).

<sup>2</sup>[www.tug.tubitak.gov.tr](http://www.tug.tubitak.gov.tr)

**Table 2** Log of observations, with exposure times for each passband. *N* denotes the number of exposure.

Filter	Exp. time (s)×N
<i>U</i>	360×3, 600×3
<i>B</i>	90×5, 360×3
<i>V</i>	20×5, 90×5, 360×3

For pre-reduction processes and transforming the pixel coordinates to equatorial coordinates, Image Reduction and Analysis Facility (IRAF)<sup>3</sup> routines, PyRAF<sup>4</sup>, and astrometry.net<sup>5</sup> (Lang et al. 2009) software were used together with custom written python scripts. Several standard stars selected from Landolt (2009) were also observed during the night to determine the atmospheric extinction and transformation coefficients of the observing system. IRAF software packages for aperture photometry were used to measure the instrumental magnitudes of the standard stars. Source Extractor (SExtractor)<sup>6</sup> and PSF Extractor (PSFEx) (Bertin & Arnouts 1996; Bertin 2011) together with custom written python and IDL scripts were used to detect and measure fluxes of all the objects in the field of the cluster and create final source catalogs. Also aperture photometry of a number of well separated stars in the field was performed, in order to make aperture corrections to the instrumental magnitudes obtained from PSF photometry. Finally, the following equations (Janes & Hoq 2011; Janes et al. 2013) were used to transform the instrumental magnitudes and colours of stars to the standard photometric system:

$$V = v - \alpha_{bv}(B - V) - k_v X_v - C_{bv} \quad (1)$$

$$B - V = \frac{(b - v) - (k_b - k_v)X_{bv} - (C_b - C_{bv})}{\alpha_b + k'_b X_b - \alpha_{bv}} \quad (2)$$

$$U - B = \frac{(u - b) - (1 - \alpha_b - k'_b X_b)(B - V)}{\alpha_{ub} + k'_u X_u} - \frac{(k_u - k_b)X_{ub} - (C_{ub} - C_b)}{\alpha_{ub} + k'_u X_u} \quad (3)$$

where *U*, *B* and *V* denote the magnitudes in the standard photometric system, *u*, *b* and *v* the instrumental magnitudes and *X* the airmass. *k* and *k'* are primary and secondary extinction coefficients while  $\alpha$  and *C* are transformation coefficients to the standard system. The photometric extinction and transformation coefficients for that particular night were obtained applying multiple linear fits to the instrumental magnitudes of the standard stars. The resulting values are given in Table 3.

<sup>3</sup>IRAF is distributed by the National Optical Astronomy Observatories

<sup>4</sup>PyRAF is a product of the Space Telescope Science Institute, which is operated by AURA for NASA

<sup>5</sup><http://astrometry.net>

<sup>6</sup>SExtractor: Software for source extraction

**Table 3** Derived transformation and extinction coefficients.  $k$  and  $k'$  denote primary and secondary extinction coefficients, respectively, while  $\alpha$  and  $C$  are transformation coefficients.

Band/Coefficient	$k$	$k'$	$\alpha$	$C$
$u$	$0.429 \pm 0.053$	$-0.240 \pm 0.084$	-	-
$b$	$0.229 \pm 0.058$	$0.082 \pm 0.061$	$0.741 \pm 0.097$	$1.496 \pm 0.092$
$v$	$0.199 \pm 0.009$	-	-	-
$u - b$	-	-	$1.119 \pm 0.123$	$3.852 \pm 0.081$
$b - v$	-	-	$0.055 \pm 0.016$	$1.345 \pm 0.026$

**Table 4** Photometric and astrometric catalogue for the open cluster NGC 6819. The complete table can be obtained electronically.

ID	$\alpha_{2000}$ (hh:mm:ss.ss)	$\delta_{2000}$ (dd:mm:ss.ss)	$V$ (mag)	$U - B$ (mag)	$B - V$ (mag)	$\mu_{\alpha} \cos \delta$ (mas yr <sup>-1</sup> )	$\mu_{\delta}$ (mas yr <sup>-1</sup> )	$P$ (%)
1	19:40:24.59	40: 3:18.58	20.440±0.046	-	1.496±0.111	-8.5±5.5	-2.2±5.5	85
2	19:40:24.65	40: 9:40.85	18.709±0.010	0.211±0.060	0.753±0.018	-0.6±7.8	-0.7±7.8	94
3	19:40:24.66	40: 9:58.24	19.883±0.026	-	1.484±0.068	-105.1±6.2	-171.7±6.2	0
4	19:40:24.73	40:13:41.68	20.387±0.041	-	1.536±0.110	-	-	-
5	19:40:24.75	40: 7: 4.94	18.102±0.006	0.540±0.052	0.939±0.012	2.0±4.0	1.5±4.0	44
-	-	-	-	-	-	-	-	-
-	-	-	-	-	-	-	-	-
-	-	-	-	-	-	-	-	-

### 3 Data analysis

#### 3.1 Identification of stars and photometric errors

In the field of NGC 6819, we identified 7382 sources and constructed a photometric and astrometric catalogue. We used the stellarity index (SI) provided by SExtractor to detect non-stellar objects, most likely galaxies, in this catalogue. A source with the SI close to 1 is a point source (most likely a star), while an extended object has an SI close to zero (Bertin & Arnouts 1996). Andreuzzi et al. (2002) and Karaali et al. (2004) showed that the objects with an SI smaller than 0.8 can be assumed to be extended objects. We adopted this limit, to determine objects which are most likely stars. Resulting catalogue contains 7060 stars and is given in Table 4. The columns of the table are organized as ID, equatorial coordinates, apparent magnitude ( $V$ ), colours ( $U - B$ ,  $B - V$ ), proper motion components ( $\mu_{\alpha} \cos \delta$ ,  $\mu_{\delta}$ ) and the probability of membership ( $P$ ). The proper motions of the stars were taken from the astrometric catalogue of Roeser et al. (PPMXL; 2010).

The errors of the measurements in the  $V$  band and  $U - B$  and  $B - V$  colours are shown in Fig. 2 as a function of the apparent  $V$  magnitude. Mean errors in the selected magnitude ranges are listed in Table 5. The errors are relatively small for stars with  $V < 18$  mag, while they increase exponentially towards fainter magnitudes. As expected, the largest errors for a given  $V$  magnitude occur in the  $U - B$  colours of the stars.

For stars brighter than  $V = 16$  mag and stars with  $V$  magnitudes between 16 and 19, the mean photometric errors in the  $B - V$  colour are smaller than 0.005 and 0.016 mag, respectively. For the same  $V$  band intervals the mean errors in the  $U - B$  colour index are smaller than 0.009 and 0.065 mag, respectively.

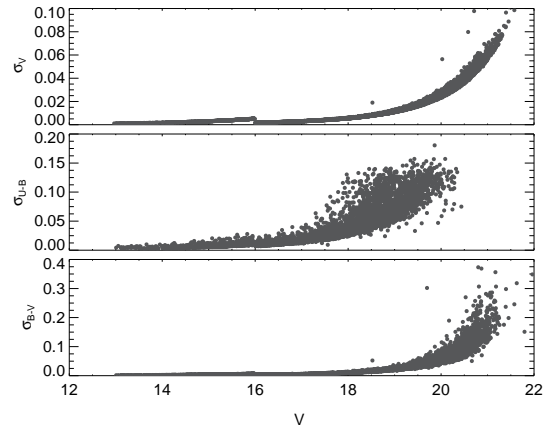


**Fig. 2** Colour and magnitude errors of the stars observed in the line-of-sight of the open cluster NGC 6819, as a function of  $V$  apparent magnitude.

We compared our photometric measurements with those of Carraro et al. (2013), Rosvick & Vandenberg (1998) and Yang et al. (2013) in Fig. 3 using all the stars detected both in those observations and ours.

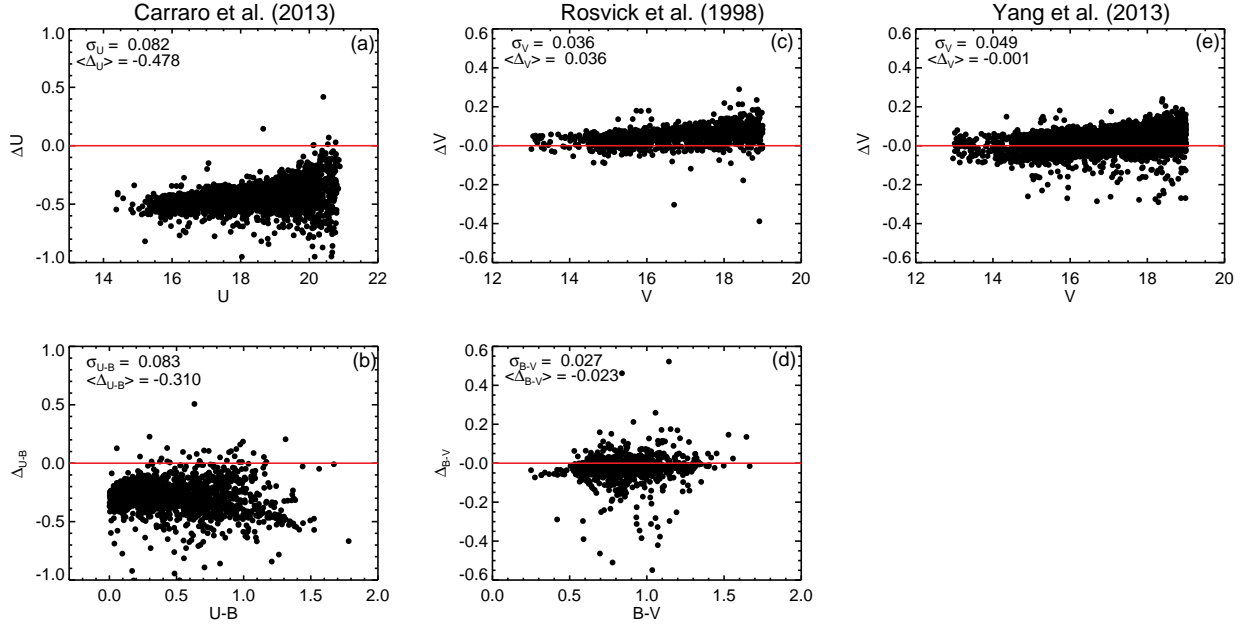


**Fig. 3** Comparison of the magnitudes and colours in this study with those of Carraro et al. (2013) (a and b), Rosvick & Vandenberg (1998) (c and d) and Yang et al. (2013) (e). The means and standard deviations of the differences are shown in panels.

**Table 6** Means and standard deviations of the magnitude and colour differences between this study and previous studies.

Carraro et al. (2013)		Rosvick & Vandenberg (1998)		Yang et al. (2013)	
$\langle \Delta_U \rangle$	$\sigma_U$	$\langle \Delta_{U-B} \rangle$	$\sigma_{U-B}$	$\langle \Delta_V \rangle$	$\sigma_V$
(mag)	(mag)	(mag)	(mag)	(mag)	(mag)
0.082	-0.478	0.083	-0.310	0.036	0.036
				$\langle \Delta_{B-V} \rangle$	$\sigma_{B-V}$
				(mag)	(mag)
				0.027	-0.023
				$\langle \Delta_V \rangle$	$\sigma_V$
				(mag)	(mag)
				0.049	-0.001

**Table 5** Mean errors of the photometric measurements for the stars in the direction of NGC 6819.  $N$  indicates the number of stars within the  $V$  apparent magnitude range given in the first column.

Mag. Range	$N$	$\sigma_V$	$\sigma_{U-B}$	$\sigma_{B-V}$
12 < $V$ ≤ 14	87	0.001	0.005	0.002
14 < $V$ ≤ 15	212	0.002	0.006	0.003
15 < $V$ ≤ 16	572	0.004	0.009	0.005
16 < $V$ ≤ 17	588	0.002	0.013	0.004
17 < $V$ ≤ 18	950	0.004	0.029	0.008
18 < $V$ ≤ 19	1431	0.008	0.065	0.016
19 < $V$ ≤ 20	1845	0.018	0.099	0.038
20 < $V$ ≤ 21	1332	0.037	0.150	0.093
21 < $V$ ≤ 24	43	0.120	—	0.212

In Fig. 3, values on the abscissae refer to our measurements, while the magnitude or colour differences in the ordinates present the differences between the two catalogues. Mean differences and standard deviations obtained for each of the five panels are also

listed in Table 6. As evident from Fig. 3, a good agreement is found from the comparison of our measurements with those of Rosvick & Vandenberg (1998) and Yang et al. (2013). While, the mean magnitude and colour residuals are  $\langle \Delta_V \rangle = 0.036 \pm 0.036$  and  $\langle \Delta_{B-V} \rangle = -0.023 \pm 0.027$  mag from the comparison with Rosvick & Vandenberg (1998), the mean magnitude residual is  $\langle \Delta_V \rangle = -0.001 \pm 0.049$  mag from the comparison with Yang et al. (2013), over the whole star sample. As for the comparison with Carraro et al. (2013), differences between the two catalogues is striking for  $\Delta_U$  and  $\Delta_{U-B}$  with the mean magnitude and colour residuals of  $\langle \Delta_U \rangle = -0.478 \pm 0.082$  and  $\langle \Delta_{U-B} \rangle = -0.310 \pm 0.083$ , respectively, over the whole star sample. Note that while transforming the instrumental magnitudes to the standard system Carraro et al. (2013) did not use a  $B - V$  colour term, which may be the reason of this discrepancy. In addition, the colour excess  $E(U - B) = 0.15$  estimated in Carraro et al. (2013) is considerably higher than expected from the colour excess ( $E(B - V)$ ) values derived in the other studies (see Table 1), since the colour excess

$E(B - V)$  should be about 0.21 according to the relation  $E(U - B)/E(B - V) = 0.72$  when  $E(U - B) = 0.15$  mag.

Determination of the photometric completeness limit of the data is important to calculate reliably the astrophysical and structural parameters. In order to find the completeness limit of our observations in the  $V$  band, we constructed a histogram of  $V$  magnitudes (see. Fig. 4). From this histogram, we concluded that the completeness limit of the  $V$  magnitudes is 19 mag as this is the mode of the distribution. Thus, we decided to only use the stars with  $V \leq 19$  mag for further analysis. With this selection the number of remaining stars for the analysis is 3840 in the field of NGC 6819.

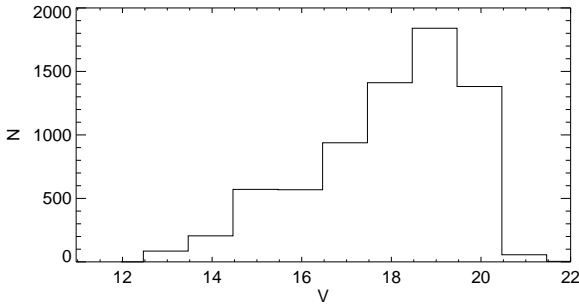


**Fig. 4** Histogram of the  $V$  magnitudes measured in the field of the open cluster NGC 6819.

### 3.2 Cluster radius and radial stellar surface density

We calculated the structural parameters of NGC 6819 by counting the number of stars in different annuli around the center of the cluster. This allowed us to estimate the stellar density profile of the open cluster NGC 6819 using 3840 stars with  $V \leq 19$  mag in the field. The central coordinates of the cluster were assumed to be as given by Yang et al. (2013) ( $\alpha_{2000.0} = 19^h 41^m 16^s.43$ ,  $\delta_{2000.0} = +40^\circ 11' 48''.88$ ). Then, the stellar density in an area defined by a circle centered on these coordinates with a radius of 1.5 arcmin was calculated. From this central circle, the variation of stellar density using annuli with widths of 1 arcmin was calculated. The last annulus had a width of 0.75 arcmin because of the decrease in the number of stars. These calculations of the stellar density were used to plot the stellar density profile in Fig. 5. We fitted the density profile in Fig. 5 with the King (1962) model defined as,

$$\rho(r) = f_{bg} + \frac{f_0}{1 + (r/r_c)^2}, \quad (4)$$

where  $r$  represents the radius of the cluster centered at the celestial coordinates given above.  $f_{bg}$ ,  $f_0$  and  $r_c$  denote the background stellar density, the central stellar density and the core radius of the cluster, respectively. In the fitting process, we used a  $\chi^2$  minimization technique to determine  $f_{bg}$ ,  $f_0$  and  $r_c$ . The best fit to the density profile is shown with a solid line in Fig. 5. From this fit, the central stellar density and core radius of the cluster, together with the background stellar density were inferred as  $f_0 = 13.18 \pm 0.46$  stars arcmin $^{-2}$ ,  $r_c = 3.65 \pm 0.38$  arcmin and  $f_{bg} = 5.98 \pm 0.45$  stars arcmin $^{-2}$ , respectively. The core radius of the cluster derived in this study compares with  $r_c = 2.80 \pm 0.17$  arcmin estimated by Yang et al. (2013). Assuming a distance of about 2.3 kpc for the cluster (see Table 1), the inferred value corresponds to a core radius of  $r_c = 2.44 \pm 0.26$  pc, which compares with the core radius of  $r_c = 1.75$  pc found by Kalirai et al. (2001).

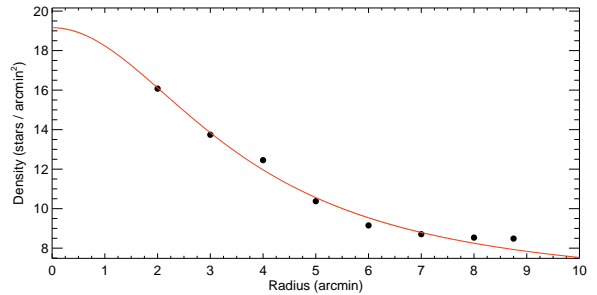


**Fig. 5** Stellar density profile of NGC 6819. Errors were determined from sampling statistics:  $1/\sqrt{N}$ , where  $N$  is the number of stars used in the density estimation.

### 3.3 CMDs and membership probabilities

We constructed  $V$  vs  $U - B$  and  $V$  vs  $B - V$  CMDs to derive the astrophysical parameters of NGC 6819. The CMDs of NGC 6819 are shown in Fig. 6. The filled circles in Fig. 6 show the 248 stars in our field of view, whose high-dispersion spectra were analyzed by Lee-Brown et al. (2015). An inspection by eye suggests that the cluster is rather dense and its main sequence and giant stars can be easily distinguished. The turn-off point including a small group of bright and blue stars in the CMDs of the cluster is located between  $V \sim 14.5$  and 15.5 mag. Location of these stars in the CMDs are very important in the age determination of the cluster.

Red clump (RC) stars can be used as standard candles for distance estimates (i.e. Paczynski & Stanek 1998; Cabrera-Lavers et al. 2005, 2007; Bilir et al. 2013a; Karaali et al. 2013) also their location on a CMD has a crucial importance in fitting the theoretical isochrones.

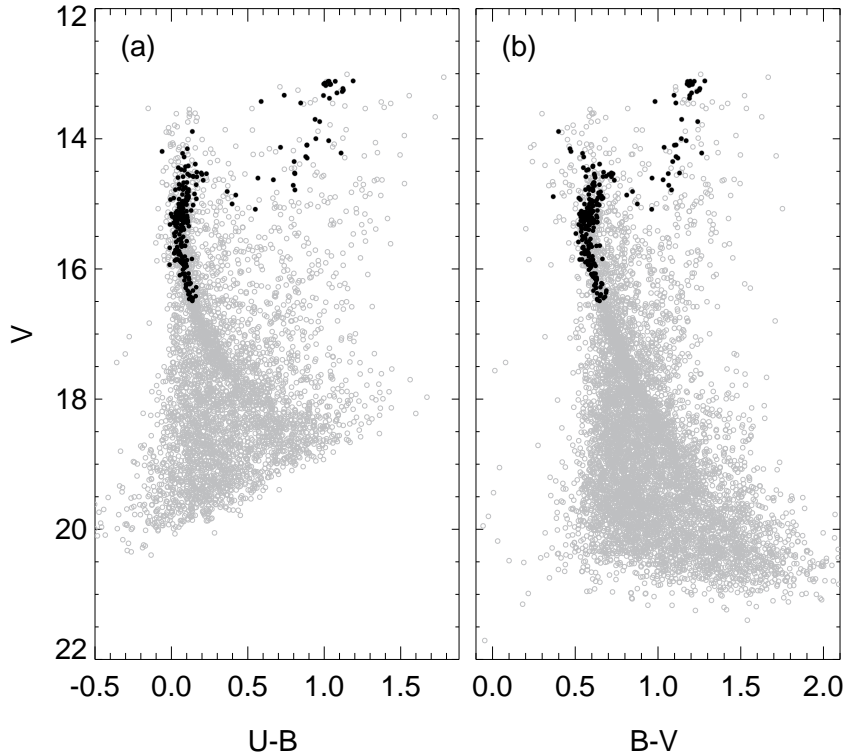


**Fig. 6** The CMDs for the cluster NGC 6819. (a)  $V$  vs  $U - B$  and (b)  $V$  vs  $B - V$ . The filled circles present the stars with the high-dispersion spectra analyzed in Lee-Brown et al. (2015)

The RC stars in CMDs of the open clusters can be used to determine the distances and ages of them, since the location of the RC stars on the  $V$  vs  $B - V$  CMD can be easily found in the colour range  $0.7 \leq (B - V)_0 \leq 1.2$  mag and the absolute magnitude range  $0 \leq M_V \leq 2$  mag (Bilir et al. 2013b). Here,  $(B - V)_0$  denotes the de-reddened  $B - V$  colour. Thus, RC stars of the open cluster NGC 6819 should be located roughly in the same colour range and between the apparent magnitudes  $V \sim 13$  and  $13.5$  of the  $V$  vs  $B - V$  CMD of NGC 6819. An inspection by eye demonstrate that there are stars in the mentioned colour and apparent magnitude ranges in Fig. 6. Once we determine membership probabilities of the stars in the direction of NGC 6819, the RC and turn-off stars can be used to confirm the distance and age estimation of the cluster.

In order to use the stars near the RC region and turn-off point of the CMDs, it should be known if they are physical members of the cluster. Moreover, NGC 6819’s main-sequence can be better determined with the identification of the likely members of the cluster. Thus, we calculated the probabilities of the stars in the field being physical members of the cluster ( $P$ ). In order to do this, we used the method described by Balaguer-Núñez et al. (1998). In this non-

parametric method, both the errors of the mean cluster and the stellar proper motions are taken into account, and the cluster and field stars’ distributions are empirically determined without any assumption about their shape. The kernel estimation technique (with a circular Gaussian kernel function) was used to derive the data distributions. The proper motions of the stars were taken from Roeser et al. (2010). In order to compare our results with those of the algorithm published by Javakhishvili et al. (2006), we considered rectangular coordinates of the stars in the field, measured in two epochs, first of our observations and second the ones obtained from Roeser et al. (2010). Consequently, we found excellent agreement. The histogram of the differences efficiently discriminate the members of the cluster from the non-members.

The next step is the determination of the most likely members of NGC 6819. For this purpose, we first selected the stars in a circle with a radius of 6 arcmin whose centre coincides with the cluster’s centre. The selected radius of 6 arcmin corresponds to roughly two times the core radius of NGC 6819, beyond which the field stars are dominant, as can be seen from Fig. 5. This circle includes 2345 stars within our catalogue.

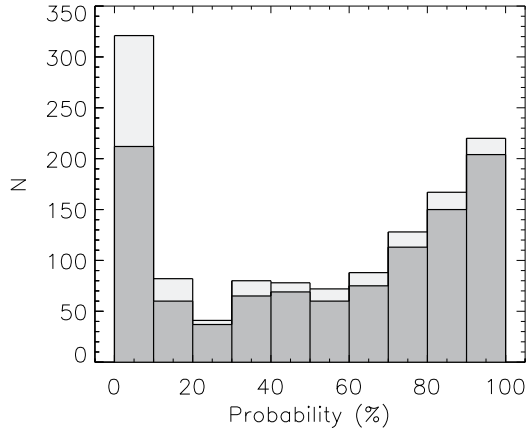


**Fig. 7** The histogram of the membership probabilities of the stars in a circle with a radius of 6 arcmin whose centre coincides with NGC 6819’s centre for  $12 \leq V \leq 19$  (light shaded bars) and  $15.5 \leq V \leq 19$  mag (shaded bars), respectively.

Fig. 7 shows the histogram of the membership probabilities of the stars in the selected radius for  $12 \leq V \leq 19$  and  $15.5 \leq V \leq 19$  mag, respectively. Here, as noted above, the magnitude  $V = 15.5$  roughly corresponds to the turn-off point of the cluster, while  $V = 19$  mag is the photometric completeness limit of our measurements. From the histograms in Fig. 7, we conclude that the stars with  $P \geq 50\%$  are likely members of the cluster. We then fitted the zero age main-sequence (ZAMS) of Sung et al. (2013) for solar metallicity to the  $V$  vs  $B - V$  CMD of NGC 6819 for  $15.5 \leq V \leq 19$  mag using only the stars with  $P \geq 50\%$  in order to identify the main-sequence stars of the cluster. Note that these stars are also located in the circle defined above. By shifting the fitted main-sequence to brighter  $V$  magnitudes by 0.75 mag, a band like region in  $V$  vs  $B - V$  CMD was obtained, as well. Hence, we assumed that all stars with a membership probability  $P \geq 50\%$  and located within the band-like region defined above are the most likely main-sequence members of NGC 6819, resulting 299 stars. A visual inspection demonstrate that the stars brighter than  $V = 15.5$  mag already left the ZAMS. Thus, we conclude that this magnitude indeed roughly corresponds to the turn-off point of the cluster. Hence, we assumed that all stars brighter than  $V = 15.5$  mag, which are also located in the circle defined above and have a probability of membership larger than  $P = 50\%$ , are the most likely members of the cluster (74 stars). With this procedure, we identified 373 stars for further analyses which are indicated with red dots in Fig. 8.

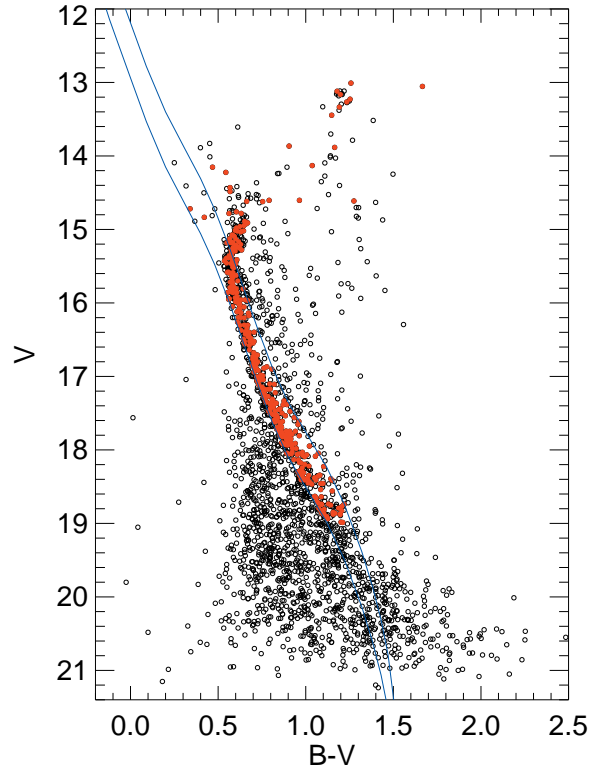


**Fig. 8**  $V$  vs  $B - V$  CMD of NGC 6819 constructed using stars which are located in a circle of 6 arcmin radius from the centre of the cluster. Solid lines represent the ZAMS of Sung et al. (2013) and the one shifted by an amount of 0.75 mag to the bright  $V$  magnitudes. Red dots indicate the most probable cluster stars that are identified using a procedure explained in the text.

## 4 Determination of the astrophysical parameters of NGC 6819

### 4.1 The reddening

Reddening of the cluster is the first parameter that must be estimated since it effects the two-colour diagram (TCD) and CMDs, from which the remaining astrophysical parameters will be determined. For the determination of the colour excesses  $E(U - B)$  and  $E(B - V)$ , we used the most probable 299 main-sequence stars in the  $15.5 \leq V \leq 19.0$  magnitude range, which were selected according to the procedure in Section 3.3. The positions of these stars in the  $U - B$  vs  $B - V$  TCD were compared with the ZAMS of Sung et al. (2013) with a solar metallicity. In order to do this, based on the proximity parameter described in Jordi et al. (1996), we shifted the de-reddened main-sequence curve of Sung et al. (2013) with steps of 0.001 mag within the range  $0 \leq E(B - V) \leq 0.20$  mag until the best fit is



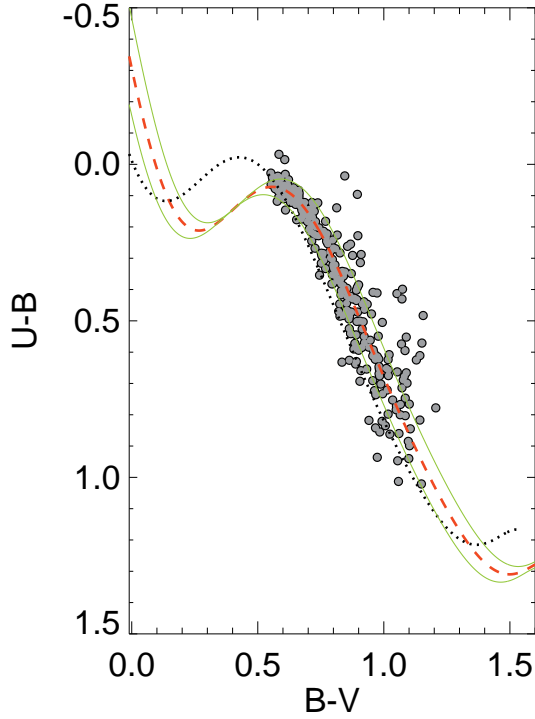


**Fig. 9**  $U - B$  vs  $B - V$  TCD for the main-sequence stars with  $15.5 \leq V \leq 19$  mag of NGC 6819. The reddened and de-reddened main-sequence curves (Sung et al. 2013) fitted to the cluster stars are represented with red dashed and black dotted lines, respectively. Green lines represent  $\pm 1\sigma$  deviations.

obtained with the  $U - B$  vs  $B - V$  TCD of NGC 6819. We calculated the shift in the  $U - B$  axis by adopting the following equation (Hiltner & Johnson 1956; Garcia et al. 1988):

$$E(U - B) = E(B - V) \times [0.72 + 0.05 \times E(B - V)]. \quad (5)$$

We show the  $U - B$  vs  $B - V$  TCD of NGC 6819 for the most probable main-sequence stars of the cluster in Fig. 9. Using this method, we estimate the following colour excesses:  $E(U - B) = 0.094 \pm 0.025$  and  $E(B - V) = 0.130 \pm 0.035$  mag. The errors were estimated by shifting the best fit curve for  $\pm 1\sigma$ .

#### 4.2 Photometric metallicity of NGC 6819

To measure the photometric metallicity of the open cluster NGC 6819, we used the method described in Karaali et al. (2011). Since this procedure uses F-G type main-sequence stars, we selected 141 of 299 stars with colours  $0.3 \leq (B - V)_0 \leq 0.6$  mag corresponding to F0-G0 spectral type main-sequence stars (Cox 2000).

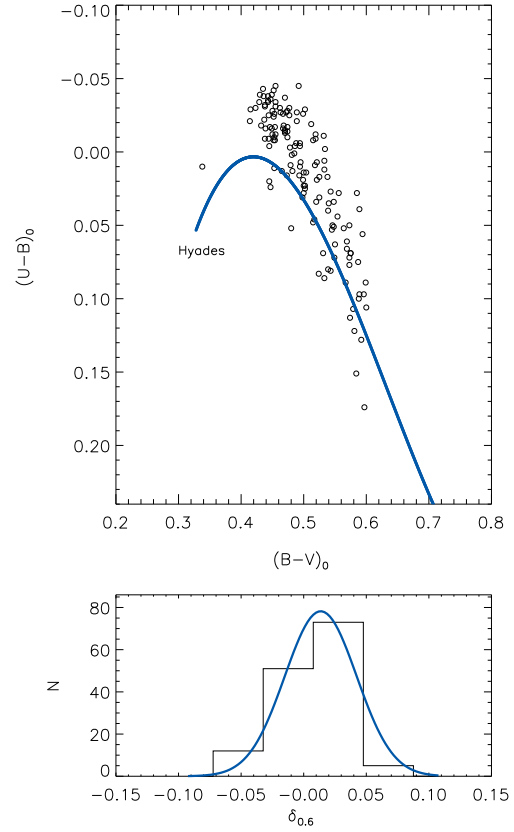


**Fig. 10** The  $(U - B)_0$  vs  $(B - V)_0$  TCD (*upper panel*) and the histogram (*lower panel*) for the normalized UV-excess for 141 main-sequence stars used for the metallicity estimation of NGC 6819. The solid lines in the upper and lower panels represent the main-sequence of Hyades cluster and the Gaussian fit of the histogram, respectively.

The normalized ultraviolet (UV) excesses of the selected stars must be calculated to utilize the method described in Karaali et al. (2011). The normalized UV excess of a star is defined as the difference between its de-reddened  $(U - B)_0$  colour indice and the one corresponding to the members of the Hyades cluster with the same de-reddened  $(B - V)_0$  colour index, i.e.  $\delta = (U - B)_{0,H} - (U - B)_{0,S}$ . Here, the subscripts  $H$  and  $S$  refer to Hyades and star, respectively. Therefore, we calculated the normalized UV excesses of the 141 stars selected as described above and normalized their  $\delta$  differences to the UV-excess at  $(B - V)_0 = 0.6$  mag, i.e.  $\delta_{0.6}$ .

Fig. 10 shows the  $(U - B)_0$  vs  $(B - V)_0$  TCD and the histogram of the normalized  $\delta_{0.6}$  UV excesses of the selected 141 main-sequence stars of NGC 6819. We calculated the normalized UV excess as  $\delta_{0.6} = 0.014 \pm 0.002$  mag by fitting a Gaussian to this histogram, which is

also shown in Fig. 10. Here, the uncertainty is given as the statistical uncertainty of the peak of the Gaussian. Then, we estimated the metallicity ( $[Fe/H]$ ) of the cluster by evaluating this Gaussian peak value in the following equation of Karaali et al. (2011):

$$[Fe/H] = -14.316(1.919)\delta_{0.6}^2 - 3.557(0.285)\delta_{0.6} + 0.105(0.039). \quad (6)$$

The metallicity corresponding to the peak value for the  $\delta_{0.6}$  distribution was calculated as  $[Fe/H] = +0.051 \pm 0.020$  dex. The error value of the metallicity was estimated due to the stated errors in the colour excess  $E(B - V)$  by assuming a colour excess that is  $1\sigma$  higher and  $1\sigma$  lower and then calculating  $[Fe/H]$  in each case.

The following relation to transform the  $[Fe/H]$  metallicities obtained from the photometry to the mass fraction  $Z$  (Mowlavi et al. 2012):

$$Z = \frac{0.013}{0.04 + 10^{-[Fe/H]}}. \quad (7)$$

Here,  $Z$  is the mass fraction of all elements heavier than helium, which is used to estimate the theoretical stellar evolutionary isochrones. Hence, we calculated  $Z = 0.011 \pm 0.002$  from the metallicity ( $[Fe/H] = +0.051 \pm 0.020$  dex) obtained from the photometry. Since this abundance is very close to the solar value, which is given as  $Z = 0.0152$  by Bressan et al. (2012), we prefer to use the solar abundance in the determination of the astrophysical parameters of the cluster.

In order to compare the photometric and spectroscopic metallicities, we selected the F0-G0 type main-sequence stars in the sample given by Lee-Brown et al. (2015), who analyzed high-dispersion spectra of 333 stars in the field of NGC 6819 to determine the abundances of iron and other metals and found the cluster's metallicity to be  $[Fe/H] = -0.02 \pm 0.02$  dex using a subsample restricted to main-sequence and turnoff stars. We identified 141 F0-G0 type main-sequence stars in their sample, for which the mod value of the metallicities is  $[Fe/H] = +0.025$  dex, which is in agreement with the metallicity of  $[Fe/H] = +0.051 \pm 0.020$  dex in this study.

#### 4.3 Distance modulus and age of NGC 6819

We already measured the reddening and metallicity of the cluster using its  $(U - B)_0$  vs  $(B - V)_0$  TCD and the normalized ultraviolet (UV) excesses of the cluster members, respectively. In order to derive the distance modulus and age of NGC 6819 simultaneously,

we fitted the CMDs of the cluster with the theoretical isochrones provided by the PARSEC synthetic stellar library (Bressan et al. 2012), which was recently updated (PARSEC version 1.2S, Tang et al. 2014; Chen et al. 2014). The metallicity and the reddening of the cluster were kept constant during the fitting process. As already noted, large uncertainties in the measured reddening, metallicity, and therefore the age values are marked due to the degeneracies between the parameters when these parameters are determined simultaneously. Thus, we ensured that the degeneracy/indeterminacy of the parameters will be less than that in the statistical solutions with four free astrophysical parameters (i.e. the metallicity, reddening, distance modulus and age) by keeping the metallicity and reddening of the cluster as constants. In Fig. 11, we overplot the best fit theoretical isochrones for  $Z = 0.0154$  and  $t = 2.4$  Gyr in the  $V$  vs  $B - V$  and  $V$  vs  $U - B$  CMDs. The estimated astrophysical parameters of NGC 6819 obtained from the best fits to the CMDs are given in Table 7. Errors of the parameters were derived by visually shifting the theoretical isochrones to include all the main-sequence stars in the CMDs.

#### 4.4 Distance via the Red Clump Stars

In order to confirm the distance estimate of the cluster given above, we utilized the red clump (RC) stars identified in the CMDs since the RC stars can be used as standard candles in distance estimation of the objects associated with them (cf. Alves 2000; Grocholski & Sarajedini 2002; Groenewegen 2008; Yaz Gökçe et al. 2013; Bilir et al. 2013a,b). Because the absolute magnitude of the RC stars are metallicity dependent especially in the optical bands, Bilir et al. (2013a) developed a  $V$ -band absolute magnitude calibration for the RC stars based on their  $B - V$  colour and metallicity using the RC stars detected in a number of stellar clusters, as following,

$$M_V = 0.627(\pm 0.104)(B - V)_0 + 0.046(\pm 0.043)[Fe/H] + 0.262(\pm 0.111), \quad (8)$$

The calibration equation is valid in the ranges  $0.42 < (B - V)_0 < 1.20$  mag,  $-1.55 < [Fe/H] < +0.40$  dex and  $0.43 < M_V < 1.03$  mag.

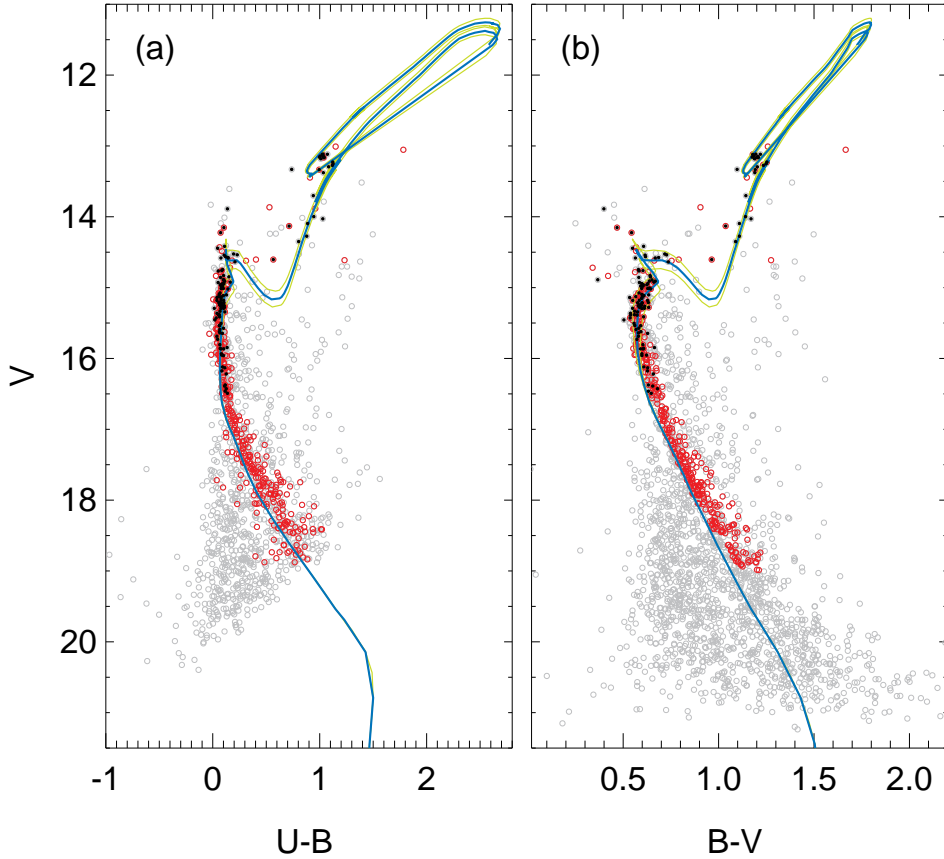
The RC stars in the  $V$  vs  $B - V$  CMD of NGC 6819 occupy a region which is limited with  $1.05 \leq B - V \leq 1.35$  and  $13.0 \leq V \leq 13.5$ . This region is indicated with a box in Fig. 12a and includes 19 stars. Seven of these stars with  $P \geq 50\%$  are denoted with red

**Table 7** Colour excesses, metallicities ( $Z$ ), distance moduli ( $\mu$ ), distances ( $d$ ) and ages ( $t$ ) estimated using two CMDs.

CMD	Colour Excess (mag)	$Z$	$\mu_V$ (mag)	$d$ (pc)	$t$ (Gyr)
$V$ vs $U - B$	$E(U - B) = 0.094 \pm 0.025$	0.0152	$12.22 \pm 0.10$	$2309 \pm 106$	$2.4 \pm 0.2$
$V$ vs $B - V$	$E(B - V) = 0.130 \pm 0.035$	0.0152	$12.22 \pm 0.10$	$2309 \pm 106$	$2.4 \pm 0.2$

**Table 8** The RC stars with a membership probability  $P \geq 50\%$  in the field of NGC 6819. ID number, equatorial coordinates,  $V$  magnitude,  $B - V$  colour and the membership probability of the stars were taken from the main photometric catalogue in this study. The  $J$ -band magnitudes were taken from the 2MASS All-Sky Catalog of Point Sources (Cutri et al. 2003). Absolute magnitudes were estimated using the calibration given by (Bilir et al. 2013a).

ID	$\alpha_{2000}$ (hh:mm:ss.ss)	$\delta_{2000}$ (dd:mm:ss.ss)	$V$ (mag)	$J$ (mag)	$B - V$ (mag)	$P$ (%)	$M_V$ (mag)	$d$ (pc)
1417	19:40:50.24	+40:13:10.92	13.120±0.001	11.009±0.020	1.179±0.002	51	0.922	2286±39
1858	19:40:57.06	+40:10:06.93	13.335±0.001	11.155±0.020	1.192±0.002	85	0.930	2514±42
1930	19:40:57.89	+40:13:53.17	13.009±0.001	10.775±0.020	1.258±0.002	95	0.972	2123±36
2761	19:41:09.30	+40:14:43.64	13.164±0.001	11.005±0.020	1.198±0.002	52	0.934	2320±40
3024	19:41:13.17	+40:06:42.04	13.446±0.001	11.374±0.020	1.148±0.002	93	0.903	2680±45
4586	19:41:33.31	+40:12:35.05	13.228±0.001	10.935±0.021	1.253±0.002	74	0.968	2351±40
4837	19:41:36.82	+40:09:03.31	13.266±0.001	10.998±0.021	1.234±0.002	98	0.957	2406±40

**Fig. 11**  $V$  vs  $B - V$  and  $V$  vs  $U - B$  CMDs for the stars located in a circle of 6 arcmin radius from the centre of NGC 6819. The most probable members of the cluster are indicated with red circles. These stars are fitted to the isochrone determined in this study (blue line). The green lines indicate the isochrones with estimated age plus/minus its error. Stars indicated with black dots are the ones with high-dispersion spectra analyzed in Lee-Brown et al. (2015).

circles in Fig. 12. We constructed the  $V_0$  vs  $J_0$  two-magnitude diagram of these RC candidate stars in order to find whether they lie in the giant region defined in Bilir et al. (2006a). Here  $J$  denotes the  $J$ -band apparent magnitude in the Two Micron All Sky Survey (2MASS; Skrutskie et al. 2006) photometric system. The equation set given by Bilir et al. (2008) was used to estimate the de-reddened  $J_0$  magnitude. Indeed, positions of the selected stars in the associated diagram (Fig. 12b) suggest that they are evolved stars (see also, Bilir et al. 2006b, 2010, 2011). We estimated their distances adopting the absolute magnitude calibration given above (Bilir et al. 2013a), and using the metallicity  $[Fe/H] = +0.051 \pm 0.020$  dex and colour excess  $E(B - V) = 0.130 \pm 0.035$  mag found in this study. Resulting distances for the RC stars are given in Table 8. The mean distance of the RC stars in Table 8 is  $d = 2383 \pm 177$  pc in agreement with the distance obtained from the theoretical isochrone fits in Table 7,  $d = 2309 \pm 106$  pc. The error value given for the mean distance obtained from the RC stars is the standard deviation of the individual distance estimates of the stars. Thus, we confirm the distance of the cluster estimated by the procedure in Section 4.3 via seven RC stars of the cluster.

#### 4.5 Galactic orbit of the cluster

We estimated the parameters of the galactic orbit of the cluster following the procedure described in Dinescu et al. (1999), Coşkunoglu et al. (2012) and Bilir et al. (2012). In order to estimate the parameters, we performed a test-particle integration in a Milky Way potential which consists of a logarithmic halo, a Miyamoto-Nagai potential to represent the galactic disc and a Hernquist potential to model the bulge.

To calculate the galactic orbit of an open cluster, its member stars with high membership probability should be used. Moreover, the proper motions and radial velocities of these stars must be available. Thus, we used only the stars whose membership probabilities are larger than  $P = \%90$  and already have radial velocities measurements from the high-dispersion spectra by Lee-Brown et al. (2015). The number of stars in the field of NGC 6819 satisfying these conditions is 12. However, one of them was removed from the list since it is a spectroscopic binary, reducing the number to 11. The data collected for these stars are listed in Table 9. The columns of the Table 9 are organized as WOCS ID, ID in our study, equatorial coordinates, apparent magnitude ( $V$ ), colour ( $B - V$ ), proper motion components ( $\mu_\alpha \cos \delta$ ,  $\mu_\delta$ ), radial velocity ( $V_r$ ) and

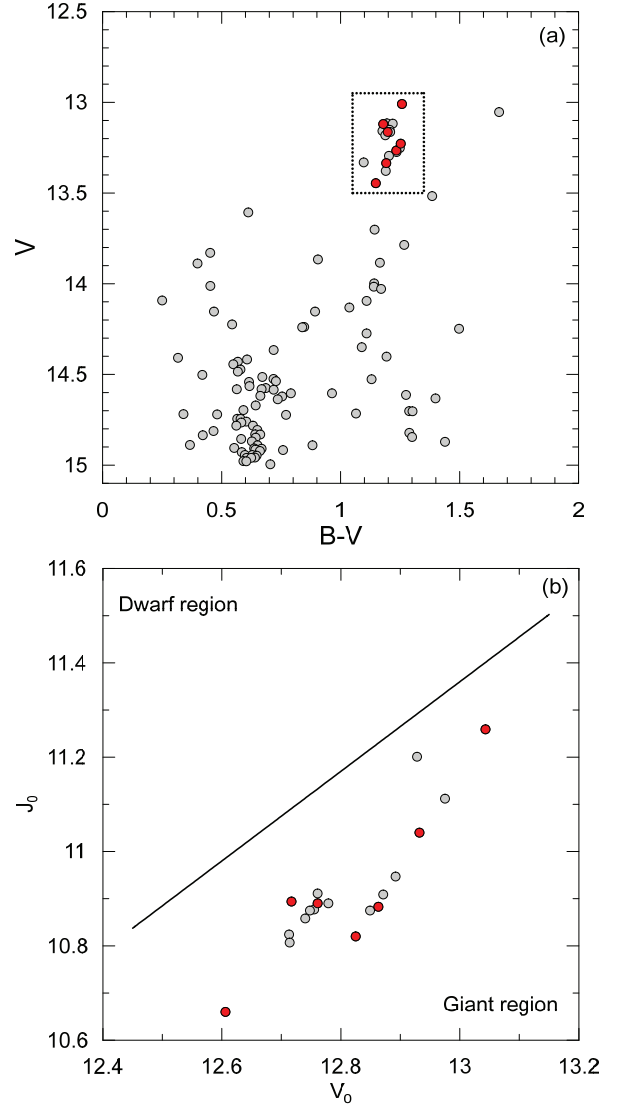


**Fig. 12** Location of the RC stars in the  $V$  vs  $B - V$  CMD of NGC 6819 indicated with a box (a) and their positions in the  $J_0$  vs  $V_0$  two-magnitude diagram (b). The solid line,  $J_0 = 0.957 \times V_0 - 1.079$ , separates the stars into dwarf and giant categories (Bilir et al. 2006a). The red circles indicate the seven RC stars with  $P \geq 50\%$  in both panels.

**Table 9** The data for stars used in the calculation of the galactic orbit of NGC 6819.

WOCS	ID	$\alpha_{2000}$ (hh:mm:ss.ss)	$\delta_{2000}$ (dd:mm:ss.ss)	$V$ (mag)	$B - V$ (mag)	$\mu_\alpha \cos \delta$ (mas yr $^{-1}$ )	$\mu_\delta$ (mas yr $^{-1}$ )	$V_r$ (km s $^{-1}$ )	$P$ (%)
28012	1806	19:40:56.46	+40:07:40.96	15.412±0.004	0.607±0.005	-4.1±3.9	-2.9±3.9	2.3±1.1	100
18013	1885	19:40:57.37	+40:16:27.48	14.760±0.003	0.604±0.003	-4.4±3.9	-1.8±3.9	3.4±1.2	97
60012	2275	19:41:02.67	+40:16:31.95	16.462±0.002	0.632±0.004	-3.2±4.1	-2.2±4.1	2.0±1.5	98
43009	2486	19:41:05.51	+40:08:28.59	15.858±0.005	0.607±0.006	-4.9±3.9	-0.7±3.9	0.7±1.6	90
25005	2517	19:41:05.87	+40:12:30.34	15.295±0.004	0.598±0.004	-3.4±3.8	-2.4±3.8	3.1±1.1	98
35008	3078	19:41:13.94	+40:15:30.31	15.639±0.004	0.580±0.005	-2.0±3.9	-4.7±3.9	3.8±1.7	92
22007	3369	19:41:17.86	+40:15:11.56	15.019±0.003	0.645±0.004	-3.4±3.8	-4.9±3.8	2.8±1.1	96
24007	4028	19:41:26.18	+40:14:36.72	15.130±0.003	0.600±0.004	-3.8±6.6	0.9±6.6	2.9±3.4	91
25008	4774	19:41:35.86	+40:10:27.72	15.388±0.004	0.573±0.005	-5.5±5.1	-1.9±5.1	-0.2±1.1	96
39009	4913	19:41:38.02	+40:10:50.26	15.805±0.005	0.604±0.006	-3.7±3.9	-0.7±3.9	2.9±1.0	90
31011	5435	19:41:45.27	+40:10:54.17	15.687±0.004	0.580±0.005	-3.8±3.9	-2.1±3.9	3.9±1.5	98

the probability of membership ( $P$ ). The proper motions of the stars were taken from the astrometric catalogue of Roeser et al. (2010). Mean values of the input parameters for the cluster’s galactic orbit estimation were obtained from Table 9:  $V_r = 2.51 \pm 1.48$  km s $^{-1}$ ,  $\mu_\alpha \cos \delta = -3.84 \pm 4.25$  and  $\mu_\delta = -2.13 \pm 4.25$  mas yr $^{-1}$ , and  $d = 2309 \pm 106$  pc, respectively. The distance of stars was assumed to be the value found in this study (see Section 4.3). Wu et al. (2009) used almost the same parameters ( $\mu_\alpha \cos \delta = -3.14 \pm 1.01$ ,  $\mu_\delta = -3.34 \pm 1.01$  mas yr $^{-1}$  and  $V_r = 4.8 \pm 0.9$  km s $^{-1}$ ) to calculate the parameters of the galactic orbit of the cluster. Galactic orbit of the cluster was determined within an integration time of 3 Gyr in steps of 2 Myr. With this integration time, the cluster completes minimum 12 revolutions around the galactic center. Thus, the averaged orbital parameters can be determined reliably. We also determined the galactic orbits of the cluster stars in Table 9.

Representations of galactic orbits calculated for the selected cluster stars and the cluster itself in the  $X - Y$  and  $X - Z$  planes are shown in Fig. 13. In Fig. 13,  $X$ ,  $Y$  and  $Z$  are heliocentric galactic coordinates directed towards the galactic centre, galactic rotation and the north galactic pole, respectively.

The cluster’s apogalactic ( $R_{max}$ ) and perigalactic ( $R_{min}$ ) distances were obtained as 8.42 and 7.50 kpc, respectively. The maximum vertical distance from the galactic plane is calculated as  $Z_{max} = 580$  pc. When determining the eccentricity projected on to the galactic plane, the following formula was used:  $e = (R_{max} - R_{min}) / (R_{max} + R_{min})$ . The eccentricity of the orbit was calculated as  $e = 0.06$ . This value shows that the cluster is orbiting the Galaxy with a period of  $P_{orb} = 142$  Myr. Although the cluster’s orbital parameters are generally in agreement with those estimated by Wu et al. (2009), the orbital period in our study is considerably

shorter than their estimate (220.5 Myr). It is not clear the origin of the difference between the orbital periods estimated in our study and that in Wu et al. (2009), while the other parameters are generally in agreement.

#### 4.6 Luminosity and mass functions of the cluster

The relative number of stars in the unit absolute magnitude range is termed as the luminosity function (LF). The problem in the estimation of the LF of an open cluster is the contamination caused by the field stars that are not physical members of the cluster. The effect of non-member stars was demonstrated in this study using the following procedure. First, we selected the turn-off and main-sequence stars with  $15.5 \leq V \leq 19$  mag located in a circular field of 6 arcmin radius from the centre of the cluster and in the band-like region as defined in Section 3.3. There are 553 stars that satisfy these conditions. Then we removed the stars whose membership probabilities could not be estimated because of the lack of proper motion measurements. This selection procedure resulted in 455 stars with the membership probability  $P > 0\%$ .

We calculated absolute magnitudes of the main-sequence stars selected with this procedure using the distance modulus  $\mu_V = 12.22 \pm 0.10$  mag in Table 7, resulting an absolute magnitude range  $3.3 \leq M_V \leq 6.8$  mag. We also calculated their masses utilizing the theoretical isochrone of the cluster. The mass range of the stars is found as  $0.765 \leq M/M_\odot \leq 1.303$  for the cluster. The LFs of NGC 6819 were estimated for the stars with the membership probabilities of  $P \geq 20\%$  ( $N = 381$ ) and  $P \geq 50\%$  ( $N = 299$ ) in order to demonstrate the effect of non-member field stars. Fig. 14 displays the LFs of the cluster.

The mass function (MF) is defined as the relative number of stars in a unit range of mass centered on

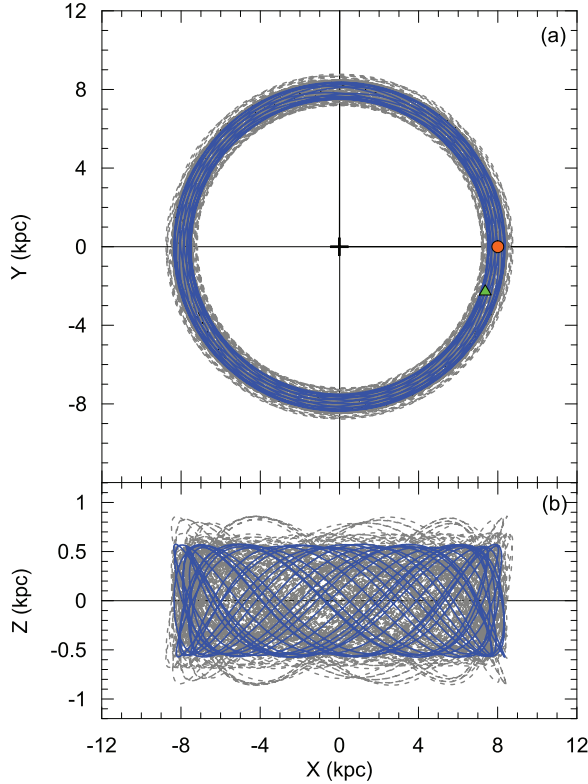


**Fig. 13** The galactic orbital motions (grey dashed lines) of the 11 cluster stars with  $P > 90\%$ , for which radial velocities are available, in the  $X - Y$  (a) and  $X - Z$  (b) planes. The cluster’s mean orbit is indicated with a blue line. The black plus, red circle and green triangle symbols in panel (a) represent the galactic centre, and current locations of the sun and NGC 6819, respectively.

mass  $M$  and represents the rate of star creation as a function of stellar mass. For NGC 6819, we used theoretical models provided by the PARSEC synthetic stellar library (Bressan et al. 2012) to convert the LFs to MFs for NGC 6819. The MFs of the cluster are shown in Fig. 15. The slope  $x$  of mass function was derived from the following linear relation:  $\log(dN/dM) = -(1+x)\log(M) + C$ , where  $dN$  represents the number of stars in a mass bin  $dM$  with central mass of  $M$ , and  $C$  is a constant. We found the slopes of the MFs to be  $x = 1.13 \pm 0.64$  and  $x = 1.70 \pm 0.78$  for the stars with the membership probabilities of  $P \geq 20\%$  and  $P \geq 50\%$ , respectively. Since these values are roughly in agreement, we conclude that the effect of non-member stars is not important for this cluster. Thus, we adopt the MF slope  $x = 1.13 \pm 0.64$  for NGC 6819. Note that this MF slope is close to the value of 1.35 given by Salpeter (1955) for the stars in the solar neighbourhood.

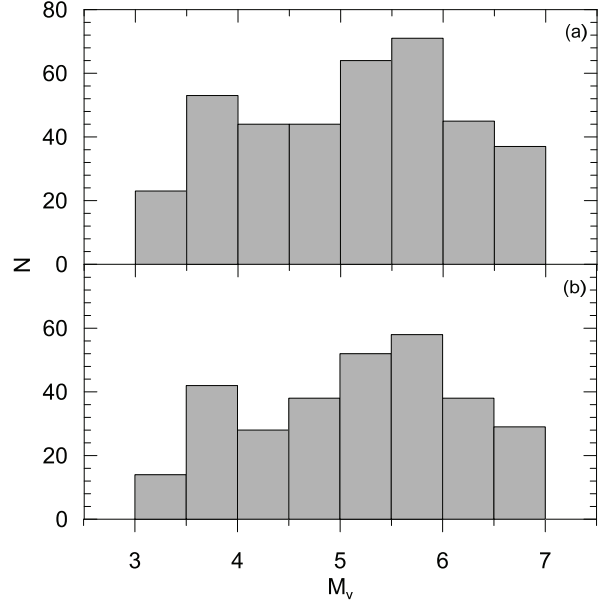


**Fig. 14** The luminosity functions of NGC 6819 estimated for the stars with the membership probability  $P \geq 20\%$  (a) and  $P \geq 50\%$  (b).

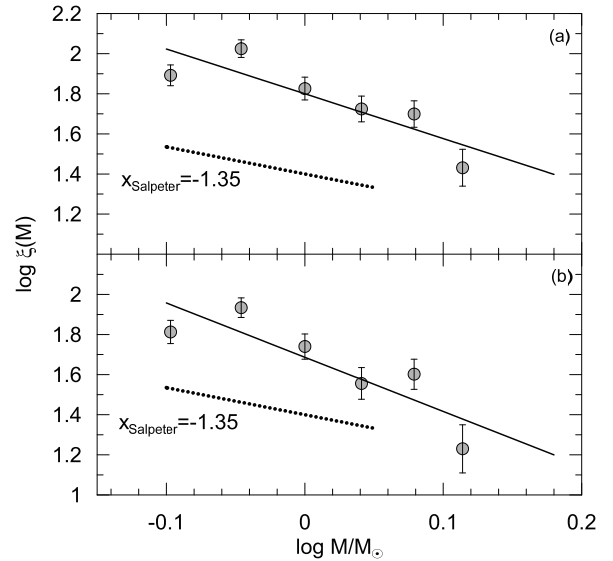


**Fig. 15** The mass functions of NGC 6819 estimated for the stars with the membership probability  $P \geq 20\%$  (a) and  $P \geq 50\%$  (b).

## 5 Conclusions

In this paper, we present CCD *UBV* photometry for the open cluster NGC 6819 and determine structural and astrophysical parameters of the cluster. The astrometric data of the stars were used to estimate their membership probabilities. Additionally, we estimated galactic orbital parameters and mass function of the cluster.

Since the astrophysical parameters of a cluster suffer from the reddening-age degeneracy when they are simultaneously determined by fitting the theoretical stellar evolutionary isochrones to the observed CMDs (cf. Anders et al. 2004; King et al. 2005; Bridżius et al. 2008; de Meulenaer et al. 2013), independent methods developed for the determination of these parameters are very promising to reduce the number of free parameters. Thus, instead of using the isochrone fits, we inferred the reddening of the open cluster NGC 6819 from its  $U - B$  vs  $B - V$  TCD, while we determined the metallicity of the cluster utilizing F0-G0 spectral type main-sequence stars (Cox 2000) via a metallicity calibration defined by Karaali et al. (2011). The metallicity obtained from the photometry is in agreement with the one inferred from the spectroscopic observations (Lee-Brown et al. 2015) and is close to the solar value. Therefore, we assumed the metallicity of the cluster to be the solar value and derived the distance modula and age of NGC 6819 by fitting the theoretical isochrones to the observed CMDs keeping the metallicity and reddening fixed. This method allows us to break in part the reddening-age degeneracy.

A comparison of Tables 1 and 6 reveals that the reddening and metallicity obtained from the independent methods are in agreement with those reported in previous photometric and spectroscopic studies in general. The age and distance modulus of the cluster derived by fitting the theoretical isochrones with the CMDs are in agreement with previous estimates, as well. The main results can be summarized as follows:

1. The central stellar density, core radius and the background stellar density for the cluster are determined as  $f_0 = 13.18 \pm 0.46$  stars arcmin<sup>-2</sup>,  $r_c = 3.65 \pm 0.38$  arcmin and  $f_{bg} = 5.98 \pm 0.45$  stars arcmin<sup>-2</sup>, respectively.
2. The reddening of the cluster was determined as  $E(B - V) = 0.130 \pm 0.035$  mag using the  $U - B$  vs  $B - V$  TCD.
3. The metallicity of NGC 6819 is inferred as  $[Fe/H] = +0.051 \pm 0.020$  dex using the UV excesses of the F and G type main-sequence stars of the cluster. This photometric metallicity is in agreement with photometric and spectroscopic metallicities appeared in the literature, in general.

4. The distance modula, the distance and the age of NGC 6819 were derived to be  $\mu_V = 12.22 \pm 0.10$  mag,  $d = 2309 \pm 106$  pc and  $t = 2.4 \pm 0.2$  Gyr, respectively, by fitting the theoretical isochrones to the observed CMDs of the cluster. We demonstrated that the distance of the cluster is in agreement with the one estimated using only the RC stars of NGC 6819.
5. Precise kinematical data of the cluster allowed for an estimation of its galactic orbit. The cluster's apogalactic ( $R_{max}$ ) and perigalactic ( $R_{min}$ ) distances, the maximum vertical distance from the galactic plane, the orbital eccentricity projected on to the galactic plane and the orbital period were calculated as  $R_{max} = 8.42$  kpc,  $R_{min} = 7.50$  kpc,  $Z_{max} = 580$  pc,  $e = 0.06$  and  $P_{orb} = 142$  Myr, respectively.
6. The slope of the mass function for the cluster is derived as  $x = 1.13 \pm 0.64$ . This slope value is close to the value of 1.35 derived by Salpeter (1955) for the stars in the solar neighbourhood.

## 6 Acknowledgments

Authors are grateful to the anonymous referee for his/her considerable contributions to improve the paper. This work has been supported in part by the Scientific and Technological Research Council (TÜBİTAK) 113F270. Part of this work was supported by the Research Fund of the University of Istanbul, Project Numbers: 39170 and 39742. We thank to TÜBİTAK National Observatory for a partial support in using T100 telescope with project number 15AT100-738. We also thank to the on-duty observers and members of the technical staff at the TÜBİTAK National Observatory for their support before and during the observations. This project is financed by the SoMoPro II programme (3SGA5916). The research leading to these results has acquired a financial grant from the People Programme (Marie Curie action) of the Seventh Framework Programme of EU according to the REA Grant Agreement No. 291782. The research is further co-financed by the South- Moravian Region. It was also supported by the grant GP14-26115P. This work reflects only the authors views and the European Union is not liable for any use that may be made of the information contained therein. This research has made use of the WEBDA, SIMBAD, and NASA's Astrophysics Data System Bibliographic Services.

## References

- Alves, D.R.: 2000, *ApJ*, 539, 732
- Anders, P., Bissantz, N., Fritze-v. Alvensleben, & U., de Grijs, R.: 2004, *MNRAS*, 347, 196
- Andreuzzi, G., Richer, H.B., Limongi, M., & Bolte, M.: 2002, *A&A*, 390, 961
- Anthony-Twarog, B.J., Deliyannis, C.P., & Twarog, B.A.: 2014, *AJ*, 148, 51
- Auner G.: 1974, *A&AS*, 13, 143
- Balaguer-Núñez, L., Tian, K.P., & Zhao, J.L.: 1998, *A&AS*, 133, 387
- Balona, L.A., et al.: 2013, *MNRAS*, 430, 3472
- Basu, S., et al., & Smith, J.C.: 2011, *ApJ*, 729, L10
- Bedin, L.R., Salaris, M., Anderson, J., Cassisi, S., Milone, A.P., Piotto, G., King, I.R., & Bergeron, P.: 2015, *MNRAS*, 448, 1779
- Bertin, E., & Arnouts, S.: 1996, *A&AS*, 117, 393
- Bertin, E.: 2011, *ASPC*, 442, 435
- Bilir, S., Karaali, S., Güver, T., Karataş, Y., & Ak, S.: 2006a, *AN*, 327, 72
- Bilir, S., Güver, T., & Aslan M.: 2006b, *AN*, 327, 693
- Bilir, S., Ak, S., Karaali, S., Cabrera-Lavers, A., Chonis, T.S., & Gaskell, C.M.: 2008, *MNRAS*, 384, 1178
- Bilir, S., Güver, T., Khamitov, I., Ak, T., Ak, S., Coşkunoglu, K. B., Paunzen, E., & Yaz, E.: 2010, *Ap&SS*, 326, 139
- Bilir, S., Karaali, S., Ak, S., Önal, Ö., Coşkunoglu, B., & Seabroke, G. M.: 2011, *MNRAS*, 418, 444
- Bilir, S., Karaali, S., Ak, S., Önal, Ö., Dağtekin, N.D., Yontan, T., Gilmore, G., & Seabroke, G.M.: 2012, *MNRAS*, 421, 3362
- Bilir, S., Ak, T., Ak, S., Yontan, T., & Bostancı, Z. F.: 2013a, *NewA*, 23, 88
- Bilir, S., Önal, Ö., Karaali, S., Cabrera-Lavers, A., & Çakmak H.: 2013b, *Ap&SS*, 344, 417
- Borucki, W.J., et al.: 2011, *ApJ*, 728, 117
- Bostancı Z.F., Ak, T., Yontan, T., Bilir, S., Güver, T., Ak, S., Çakırlı Ö., Özdarcan, O., Paunzen, E., De Cat, P., Fu, J.N., Zhang, Y., Hou, Y., Li, G., Wang, Y., Zhang, W., Shi, J., & Wu, Y.: 2015, *MNRAS*, 453, 1095
- Bragaglia, A., et al.: 2001, *AJ*, 121, 327
- Bressan, A., Marigo, P., Girardi, L., Salasnich, B., Dal Cero, C., Rubele, S., & Nanni, A.: 2012, *MNRAS*, 427, 127
- Bridžius, A., Narbutis, D., Stonkutė, R., Deveikis, V., & Vanevičius V.: 2008, *BaltA*, 17, 337
- Burkhead, M.S.: 1971, *AJ*, 76, 251
- Cabrera-Lavers A., Garzón, F., & Hammersley, P. L.: 2005, *A&A*, 433, 173
- Cabrera-Lavers A., Bilir S., Ak S., Yaz E., & López-Corredoira M.: 2007, *A&A*, 464, 565
- Carraro, G., Buzzoni, A., Bertone, E., & Buson, L.: 2013, *AJ*, 146, 128
- Chen, Y., Girardi, L., Bressan, A., Marigo, P., Barbieri, M., & Kong, X.: 2014, *MNRAS*, 444, 2525
- Corsaro, E., et al.: 2012, *ApJ*, 757, 190
- Coşkunoglu, B., Ak, S., Bilir, S., Karaali, S., Önal, Ö., Yaz, E., Gilmore, G., & Seabroke G. M.: 2012, *MNRAS*, 419, 2844
- Cox, A. N.: 2000. *Allen's astrophysical quantities*, 4th ed. Publisher: New York: AIP Press; Springer, 2000. Edited by Arthur N. Cox. ISBN: 0387987460
- Cutri, R.M., & et al.: 2003, *2MASS All-Sky Catalog of Point Sources*, CDS/ADC Electronic Catalogues, 2246
- de Meulenaer, P., Narbutis, D., Mineikis, T., & Vanevičius, V.: 2013, *A&A*, 550, 20
- Dinescu, D.I., Girardi, T.M., & van Altena, W. F.: 1999, *AJ*, 117, 1792
- Friel, E.D., Liu, T., & Janes K.A.: 1989, *PASP*, 101, 1105
- Friel E.D. & Janes K.A.: 1993, *A&A*, 267, 75
- Garcia, B., Claria, J.J. & Levato, H.: 1988, *ApSS*, 143, 317
- Glushkova, E.V., Kulagin Yu.V., & Rastorguev A.S.: 1993, *AstL*, 19, 232
- Gosnell, N.M., Pooley, D., Geller, A.M., Kalirai, J., Mathieu, R.D., Frinchaboy P., & Ramirez-Ruiz E.: 2012, *ApJ*, 745, 57
- Grocholski, A.J., & Sarajedini, A.: 2002, *AJ*, 123, 1603
- Groenewegen, M.A.T.: 2008, *A&A*, 488, 25
- Hekker, S., et al.: 2011, *A&A*, 530, 100
- Hole, K.T., Geller, A.M., Mathieu, R.D., Platais, I., Meibom, S., & Latham D.W.: 2009, *AJ*, 138, 159
- Hiltner, W.A. & Johnson, H.L.: 1956, *ApJ*, 124, 367
- Janes K., & Hoq S.: 2011, *AJ*, 141, 92
- Janes, K., Barnes, S. A., Meibom, S., & Hoq, S.: 2013, *AJ*, 145, 7
- Janes, K., Barnes, S. A., Meibom, S., & Hoq, S.: 2014, *AJ*, 147, 139
- Javakhishvili, G., Kukhianidze, V., Todua, M., & Inasaridze, R.: 2006, *A&A*, 447, 915
- Jordi, C., Trullols, E., Galadi-Enriquez, D.: 1996, *A&A*, 312, 499
- Kalirai, J.S., et al.: 2001, *AJ*, 122, 266
- Kang, Y.-W., & Ann H.B.: 2002, *JKAS*, 35, 87
- Karaali, S., Bilir, S., & Hamzaoglu E.: 2004, *MNRAS*, 355, 307
- Karaali, S., Bilir, S., Ak, S., Yaz, E., & Coşkunoglu, B.: 2011, *PASA*, 28, 95
- Karaali, S., Bilir, S., & Yaz, Gökçe E.: 2013, *Ap&SS*, 346, 89
- King I.: 1962, *AJ*, 67, 471
- King, I.R., Bedin, L.R., Piotto, G., Cassisi, S., & Anderson, J.: 2005, *AJ*, 130, 626
- Landolt, A.U.: 2009, *AJ*, 137, 4186
- Lang, D., Hogg, D. W. Mierle, K., Blanton, M., & Roweis, S., 2010, *AJ*, 137, 1782.
- Lee-Brown, D.B., Anthony-Twarog, B.J., Deliyannis, C.P., Rich, E., & Twarog, B.A.: 2015, *AJ*, 149, 121
- Lindoff, U.: 1972, *A&AS*, 7, 497
- Miglio, A., et al.: 2012, *MNRAS*, 419, 2077
- Mowlavi, N., Eggenberger, P., Meynet, G., Ekström, S., Georgy, C., Maeder, A., Charbonnel, C., & Eyer, L.: 2012, *A&A*, 541, A41
- Paczynski, B., & Stanek, K. Z., 1998, *ApJ*, 494, L219
- Rodrigues, T.S., et al.: 2014, *MNRAS*, 445, 2758
- Roeser, S., Demleitner, M., & Schilbach, E.: 2010, *AJ*, 139, 2440
- Rosvick, J.M., & Vandenberg, D.A.: 1998, *AJ*, 115, 1516
- Salpeter, E.E.: 1955, *ApJ*, 121, 161
- Sandquist, E.L., et al.: 2013, *ApJ*, 762, 58
- Skrutskie, M.F., Cutri, R.M., Stiening, R. et al.: 2006, *AJ*, 131, 1163
- Stello, D., et al.: 2011, *ApJ*, 739, 13
- Street, R.A., et al.: 2005, *MNRAS*, 358, 795



- 
- Sung, H., Lim, B., Bessell, M.S., Kim, J.S., Hur, H., Chun, M., & Park B.: 2013, JKAS, 46, 103
- Talamantes, A., Sandquist, E.L., Clem, J.L., Robb, R.M., Balam, D.D., & Shetrone, M.: 2010, AJ, 140, 1268
- Tang, J., Bressan, A., Rosenfield, P., Slemer, A., Marigo, P., Girardi, L., & Bianchi, L.: 2014, MNRAS, 445, 4287
- Thogersen, E.N., Friel, E.D., & Fallon, B.V.: 1993, PASP, 105, 1253
- Wu, Z.-Yu, Zhou, X., Ma, J., & Du, C.-H.: 2009, MNRAS, 399, 2146
- Wu, T., Li, Y., & Hekker, S.: 2014a, ApJ, 781, 44
- Wu, T., Li, Y., & Hekker, S.: 2014b, ApJ, 786, 10
- Yang, S-C., Sarajedini, A., Deliyannis, C.P., Sarrazine, A.R., Kim, S.C., & Kyeong, J.: 2013, ApJ, 762, 3
- Yaz, Gökçe, E., Bilir, S., Öztürkmen, N. D., Duran, Ş., Ak, T., Ak, S., & Karaali, S., 2013, NewA, 25, 19
- Yontan, T., et al.: 2015, Ap&SS, 355, 267